CFD Modeling of Water Mist Systems for Suppressing Shielded fires in Enclosures Using FDS

Azad Hamzehpour[1,*], Vittorio Verda[1] and Romano Borchiellini[1]

[1]Department of Energy (DENERG), Politecnico di Torino, C.so Duca degli Abruzzi 24, 10129, Torino, Italy

Corresponding author: azad.hamzehpour@polito.it

Abstract

Despite the fact that in recent years, many researchers and engineers have been working on fire-related topics and the firefighting systems, there are still unknowns in this field due to the fire phenomenon complexity. Due to the high cost of real scale experimental tests and engineering constraints, several numerical methods have been developed in recent years to simulate fire dynamics and water mist systems. Fire Dynamics Simulator (FDS) is a powerful tool to solve Navier-Stokes equations numerically. In this work, different fire scenarios in a confined space and shielded fires are analyzed using FDS. In addition, the performance of the water-based firefighting systems is assessed to find out the capability of such systems to control or extinguish the fire. This study will also help to better understand the fire behavior and the effectiveness of water-based fire suppression systems. The shielded fires representing the car top or train or shelves in real fire scenarios will be studied. The interaction between the water droplets and the shielded fire plume is of importance while investigating the fires as the chance of reaching droplets directly to the fire is low in real scenarios. The results show that the capability of water mist system to extinguish the shielded fire is dependent on the distance between the nozzle and the obstacle and also the size and the location of the obstacle and the droplet size distribution of the water mist systems. In both early application and late application of the water mist system, the nozzle with finer droplets performed better than the nozzle with coarser droplets. It was seen that both nozzles failed to suppress the fire when the obstacle is the largest (1m×1m).

KEYWORD: water mist systems, diesel pool fires, enclosure fires, shielded fires, fire dynamics simulator

1. Introduction

Fire safety matters and active and passive fire protection systems are becoming more important nowadays due to the increasing fire incidents and hazards in different spaces such as underground infrastructures, buildings, storage units etc. Water-based fire suppression systems can be categorized into water mist and water sprinkler systems with respect to the droplet size of spray nozzles. One the most effective tools to suppress and control fires is water mist system. According to NFPA 750 [1], water mist systems can be categorized into different types with respect to a variety of parameters as depicted in Fig. 1. The selection of water mist systems is highly dependent on the application and the general conditions of the space where the system is being installed in. Water mist systems can also be recognized as the low-pressure (pressure ≤ 12.1bar), intermediate-pressure (12.1bar < pressure < 34.5bar) or high-pressure (34.5bar ≤ pressure) water mist systems.

There have been numerous research studies in the literature focusing on the performance of water mist systems in extinguishing fires. Although experimental research studies cost a lot, there have been several experimental tests analyzing the performance of water mist systems in various spaces like tunnels and enclosures. Laser-based experimental tests have also been carried out to study the water mist and nozzle characteristics. A variety of experimental techniques like laser diffraction, phase doppler particle analyzer,

image analysis has been developed to measure the droplet size distribution and to find out the optimal droplet size [2,3]. Different characteristics like Sauter Mean Diameter (SMD, D32), cone angle, discharge rate, velocity, cumulative volume diameter (CVM), volumetric median diameter (VMD, Dv,50) are usually considered to be measured conducting laser experiments. A particle/droplet Image Analyzer (PDIA) was used to measure the characteristics of water mist generated by a low-pressure twin-fluid atomizer in order to assess its capability to extinguish a small pool fire. The optimum conditions and data were obtained to increase the efficiency of water mist systems [4].

Qin and Chow [5] analyzed the performance of water mist systems on extinguishing different types of fire. In a research work, fire extinguishing time, gas concentration, cover area, droplet size distributions, fire position effects, and nozzle characteristics effects were analyzed for an enclosed space fire [6]. It was shown that the fire suppression mechanism could be improved by 1- decreasing the flow rate and the spray angle and increasing the water discharge duration, and 2- increasing the flow rate and the spray angle at the same time and decreasing the water discharge duration. In tunnel fire investigations, other parameters like the ventilation condition and the geometry of the tunnel can influence the performance of water mist systems. For instance, the effect of water mist systems and parameters like the activation time, the longitudinal velocity, the working pressure, and the K-factor of the nozzles on the smoke temperature

distribution in a tunnel was examined by Fan et al. [7] and an optimal condition of a water mist system in order to control the temperature effectively was proposed. It was proved that the longitudinal ventilation can be useful to decrease the temperature and gain the visibility [7].

Besides the experimental investigations, many researchers have focused on assessing fire suppression systems using numerical tools. In this regard, Fire Dynamics Simulator (FDS) is a popular CFD tool in the literature and too many research works have been employed FDS to simulate different fire scenarios and water mist systems [8–10]. The details about FDS will be demonstrated in the next section. In CFD modeling, it is necessary to verify and validate the results with the available theoretical and experimental data. The capability of FDS to predict the effectiveness of different water mist systems on suppressing fire in open and confined spaces was assessed by Lin et al. [11]. It was demonstrated that the pulsed water mist system can extinguish fire in a confined space in a shorter time with less water consumption.
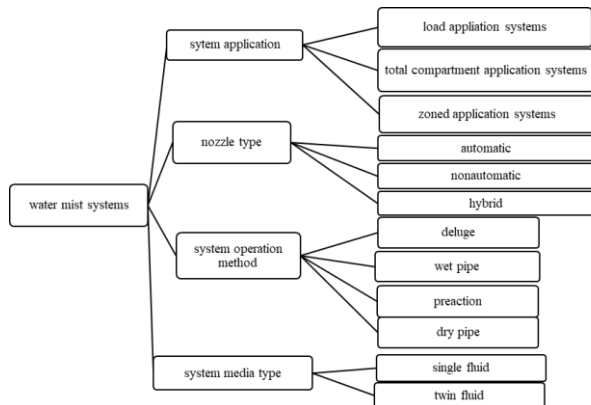

Fig 1. Classification of water mist systems with respect to different parameters [1]

In real scenarios, the existence of obstacles representing the car top in road tunnels or the roof of the trains in railways tunnels or the shelf in compartments is probable. In this case, the fire is shielded with obstacles preventing the water droplets directly reaching the fire plume.

In the studies of shielded fires suppression, it is important to investigate the fire extinguishing mechanisms and the interaction between the water droplets and the fire plume. Water mist extinguishing mechanisms can be generally classified into four parts: 1- endothermic cooling including evaporation, flame cooling, and fuel cooling and wetting 2- oxygen displacement 3- thermal radiation attenuation 4- kinetics disturbance. It should be noted that each of the aforementioned mechanisms is involved to suppress the class A and B fires to some extent [12]. In the presence of obstacles, there would be no direct fuel and flame cooling as the droplets cannot reach to the fuel surfaces. Therefore, the dominant extinguishing mechanisms in such scenarios are the

oxygen displacement and the thermal radiation attenuation. In recent years, only a few research work focused on the shielded fires and suppression of these fires by water mist systems, like [13–15]. These papers defined and used the plume-spray thrust ratio to study the interaction between the fire plume and water mist, which was previously demonstrated by Alpert [16] as the interaction between the upward fire plume thrust and the downward water mist thrust.

In this study, a low-pressure and a high-pressure water mist system will be employed to numerically investigate the capability of such systems to extinguish or control the shielded fire in an enclosure using FDS. Three different obstacle sizes, two different distances between the obstacle and the nozzle, and two different activation time are considered as the variables of this paper in addition to different nozzle characteristics. The FDS model is first validated with the experimental data. The grid sensitivity analysis is also conducted to present the grid independency of the model. The data to be evaluated include the following: the extinguishing time (in case of successful suppression), the concentrations of O_2, CO, and CO_2, the temperature and velocity fields, the HRR curve, the energy balance, and the relationship between the obstacle size, the distance from the nozzle and the extinguishing time.

2. FDS modeling

The most used models in the literature and one of the most powerful tools in simulating fires is FDS which is a CFD tool to solve the Navier-Stokes equations for low-speed flows based on Large Eddy Simulations (LES) developed by National Institute of Standards and Technology (NIST-U.S.A.) and VTT Technical Research Center of Finland [17]. In order to visualize the results after running the FDS program and for post-processing purposes, Smokeview (SMV) program is used [18]. For the mathematical representation of a fire dynamics problem, there are different approaches to discretize the governing equations, and in FDS, a finite difference method is used. There are advantages and disadvantages for every discretization method, but the finite difference method (FDM) has a fast evaluation and is of high order. The FDM is based on the evaluation of a function at certain locations and then approximation of derivatives with this data.

The combustion approach in FDS is lumped species approach meaning that three lumped species namely air, fuel, and products consisting of primitive species are transported together. The fluid dynamics in FDS, which describes the gas and liquid movement, include defining the boundary conditions, the compressibility, the turbulence modeling, the heat transfer equations, the state equation, and the chemical reactions. The fluid dynamics is based on mass, momentum, and energy conservation equations. In FDS, multiple

2

species are considered, and their masses are coupled together via source terms. Partial Differential Equations (PDEs) and in the case of FDS, Navier-stokes equations need to be solved by approximation schemes which is called CFD in general.

The mass conservation equation used in FDS is defined as follows:

$$\partial_t(\rho Z_\alpha) + \nabla.(\rho Z_\alpha \vec{v}) = \nabla.(\rho D_\alpha \nabla Z_\alpha) + \dot{m}_\alpha''' + \dot{m}_{b,\alpha}''' \qquad (1)$$

This equation represents the transport of species α by the change of mass fraction Z_α, and the sum of all mass fractions, all reaction productions, and all diffusion terms equal to zero. The momentum equation is shown below:

$$\partial_t(\rho \vec{v}) + \nabla.(\rho \vec{v}\vec{v}) = -\nabla p + \rho \vec{g} + \vec{f}_b + \nabla.\tau_{ij} \qquad (2)$$

And the energy conservation equation is defined as following:

$$\partial_t(\rho h_s) + \nabla.(\rho h_s \vec{v}) = \frac{D\bar{p}}{Dt} + \dot{q}''' + \nabla.\vec{q}'' \qquad (3)$$

Additionally, the state equation and the initial and boundary conditions are added to the above-mentioned equations to make the complete set of equations.

There are different pressure solvers in FDS including FFT, ULMAT, and GLMAT and they all have their cons and pros. The pressure can be split into background and perturbation pressures.

$$p(x,t) = \bar{p}_m(z,t) + \tilde{p}(x,t) \qquad (4)$$

In this formula, $\bar{p}_m$ is the background (thermodynamic) pressure which resolves large scale fluctuations and $\tilde{p}(x,t)$ is the perturbation (hydrodynamic) pressure which resolves the small-scale fluctuations. The full pressure equation, derived from the momentum equation can be written as follows:

$$\nabla.(\frac{1}{\rho}\nabla\tilde{p}) = -\frac{\partial(\nabla.u)}{\partial t} - \nabla.F_A - \frac{\nabla^2|u|^2}{2} \qquad (5)$$

In FDS, internal and external boundaries and mesh interface boundaries should be defined. The Dirichlet and Neumann boundary conditions are the main two types of boundary conditions. The former indicates that the value of the solution should be known at the external boundaries and the latter states that the normal gradient of the value should be known at the external boundaries. There are different pressure solvers in FDS namely Fast Fourier Transformation (FFT), ULMAT, GLMAT, UGLMAT, and UScaRC. Considering the full pressure equation mentioned

above, a simplified version of the pressure equation can be written as:

$$\nabla^2[\frac{\tilde{p}}{\rho} + \frac{|u|^2}{2}] = R_s,$$
$$[\frac{\tilde{p}}{\rho} + \frac{|u|^2}{2}] = H \qquad (6)$$

For modeling the turbulence generally in CFD, there are three main models namely RANS, LES, and DNS. In FDS, handling the turbulence is based on LES model, then there are sub models including constant and dynamic Smagorinsky, Deardorff (the default model in FDS), Vreman, and WALE which can be selected by the user.

In fire dynamics problems, the effect of the thermal radiation is not negligible and should be taken into account while solving the governing equations. In fact, in many situations, the radiation heat transfer is the dominant heat transfer mechanism in the domain. Therefore, in FDS, the Radiation Transport Equation (RTE) can be solved together with the other equations. The general equation for radiation intensity can be given by:

$$\frac{1}{c}\frac{\partial I_\lambda(x,s,t)}{\partial t} + s.\nabla I_\lambda(x,s)$$
$$= -\kappa(x,\lambda)I_\lambda(x,s) - \sigma_s(x,\lambda)I_\lambda(x,s)$$
$$+ B(x,\lambda) + \frac{\sigma_s(x,\lambda)}{4\pi}\int_{4\pi}\varphi(s',s)I_\lambda(x,\acute{s})\,d\acute{s} \qquad (7)$$

In addition, the radiation equation for a gray gas is solved using a Finite Volume Method (FVM) in FDS. The radiation solver requires a significant amount of CPU calculation time. The RadCal narrow-band model is used for calculation of the gas phase absorption coefficients.

In order to observe the effects of the shielding conditions on the fire extinguishment, a block ratio was defined and suggested by Liu et al. [13], which takes into account the impact of the obstacle size and its distance from the nozzle. As defined by Beihua et al. [15], the plume-spray thrust ratio can be written as follows:

$$\alpha = \frac{F_f}{F_w} \qquad (8)$$

Where F_f is the fire plume momentum at the nozzle location and F_w is the initial spray momentum. The following equations can be used to calculate the fire plume momentum (F_f), and the initial spray momentum (F_w) [13,15].

$$F_f = \dot{m}_p.u_0 \qquad (9)$$

$$\dot{m}_p = 0.071\dot{Q}_c^{1/3}.(z - z_0)^{5/3} + 0.00192.\dot{Q}_c \quad \text{for } z > L \qquad (10)$$

$$\dot{Q}_c = x\dot{Q} \qquad (11)$$

$$z_0 = 0.083\dot{Q}^{2/5} - 1.02D_b \qquad (12)$$

$$L = 0.235\dot{Q}^{2/5} - 1.02D_b \qquad (13)$$

$$u_0 = 1.1(\frac{z}{\dot{Q}^{2/5}})^{-1/3}.\dot{Q}^{1/5} \qquad (14)$$

$$F_w = \dot{V}.U_0 \qquad (15)$$

$$U_0 = \dot{V}.\frac{10^{-3}}{(\frac{\pi d_0^2}{4})} \qquad (16)$$

In the equations above, $\dot{m}_p$, u_0, z_0, L, U_0, $\dot{V}$ are the mass flux of plume at the nozzle location, the upward velocity of plume at the nozzle location, the height of virtual origin of fire plume, the flame height, the initial water mist droplet velocity, and the water discharge rate, respectively.

The geometry and properties of the model are obtained from the experimental data by Jenft et al. [19] The dimension of the room is 4.20 m×4.30m × 3.05 m. The parameters and the characteristics of the room used for the experimental tests and the simulation are shown in Tables below:

Tab. 1. Material properties

material	Conductivity (k) w/mk	Specific heat (cp) j/kgk	Density (ρ) kg/m³
Concrete	1.575	1000	2100
glass	1	750	2500
steel	50	450	7800
wood	0.13	1600	500

Tab. 2. Fuel properties

	Common Formula	Heat of combustion (ΔH_c) kj/kg	Soot yield kg/kg
Diesel	$C_{12}H_{23}$	42200	0.059

Several types of water mist systems and different nozzle characteristics have been used to study the effect of different parameters such as the operating pressure, the droplet size distribution, and cone angle on suppression.

As can be seen in Fig. 2, the geometry of the room is designed according to the properties mentioned in Tab. 1. For the issues related to the pressure, the computational domain is considered bigger, and the pressure zone is defined in the models. The models have all a single mesh with the total number of almost 500,000 cells (Fig. 3).
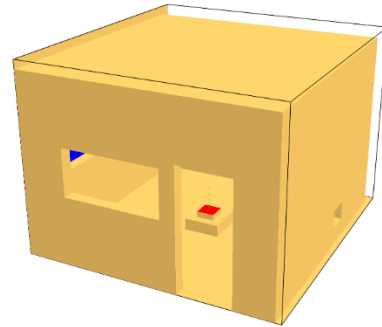

Fig 2. The geometry of the designed room in FDS
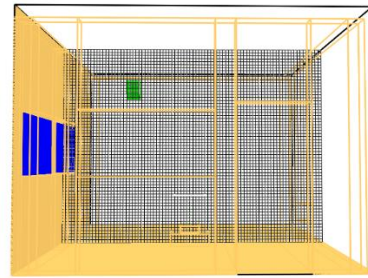

Fig 3. The grid of the designed room in FDS

In order to analyze the effectiveness of water mist systems with different nozzle characteristics to extinguish the shielded diesel fire in enclosures, a variety of input and output parameters has been considered. The variables include the size of the obstacle, the distance between the obstacle and the nozzle, the activation time of the spray, and the characteristics of the nozzle including cone angle, k factor, droplet size, operating pressure, and water discharge rate. Two nozzles with different characteristics have been considered in this work. The characteristics can be seen in Tab 3. In this paper, different cases have been defined as mentioned in Tab 4. The HRR values are the same for all cases. The variables in this study include the nozzle characteristics, the obstacle size, the location of the obstacle, and the activation time.

Tab 3. Nozzle characteristics used for simulations

Nozzle 1	Nozzle 2
D=46µm Operating pressure= 100bar Flow rate= 11.9 l/min Velocity=10 m/s Cone angle= 0-48˚	D=124.6µm Operating pressure= 10bar Flow rate= 22.8 l/min Orifice diameter=0.0025m Cone angle= 90 K factor= 7.25

Tab 4. Defined simulation cases

Case No.	HRR (kW)	Obstacle size	distance between obstacle and floor	Nozzle number	Activation time
I	75	-	-	-	-
II	75	-	-	1	75s
III	75	25cm×25cm 3mm thickness	800mm above floor	1	75s

IV	75	50cm×50cm 3mm thickness	800mm above floor	1	75s
V	75	100cm×100cm 3mm thickness	800mm above floor	1	75s
VI	75	-	-	2	75s
VII	75	25cm×25cm 3mm thickness	800mm above floor	2	75s
VIII	75	50cm×50cm 3mm thickness	800mm above floor	2	75s
IX	75	100cm×100cm 3mm thickness	800mm above floor	2	75s
X	75	25cm×25cm 3mm thickness	1500mm above floor	1	75s
XI	75	50cm×50cm 3mm thickness	1500mm above floor	1	75s
XII	75	100cm×100cm 3mm thickness	1500mm above floor	1	75s
XIII	75	25cm×25cm 3mm thickness	1500mm above floor	2	75s
XIV	75	50cm×50cm 3mm thickness	1500mm above floor	2	75s
XV	75	100cm×100cm 3mm thickness	1500mm above floor	2	75s
XVI	75	-	-	1	190s
XVII	75	25cm×25cm 3mm thickness	800mm above floor	1	190s
XVIII	75	50cm×50cm 3mm thickness	800mm above floor	1	190s
XIX	75	100cm×100cm 3mm thickness	800mm above floor	1	190s
XX	75	-	-	2	190s
XXI	75	25cm×25cm 3mm thickness	800mm above floor	2	190s
XXII	75	50cm×50cm 3mm thickness	800mm above floor	2	190s
XXIII	75	50cm×50cm 3mm thickness	800mm above floor	2	190s

3. Results and discussion

3.1. Grid sensitivity analysis

For the grid resolution study, three cases with the same characteristics except the cell size of the mesh have been considered. Three different mesh size include fine, coarse, and moderate mesh sizes. The characteristic fire diameter is calculated as the following equation suggested in the FDS user's guide [17]:

$$D^* = (\frac{\dot{Q}}{\rho_\infty c_p T_\infty \sqrt{g}})^{2/5} \qquad (17)$$

Then, the non-dimensional quantity $D^*/\delta x$ is applied to define the proper grid size for buoyant plumes simulations. For the current study, the sensitivity study is carried out by considering three different cases with coarse, moderate, and fine meshes to investigate their temperature and pressure evolution

along a vertical line lateral to the fire and at the steady state between 50s and 150s after the ignition.
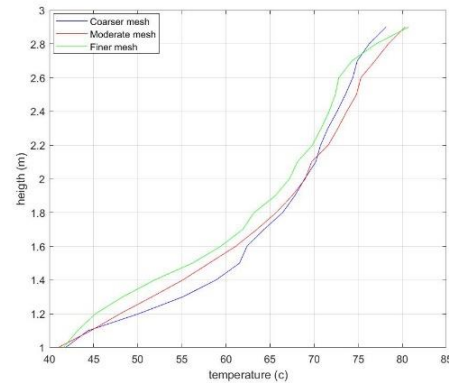

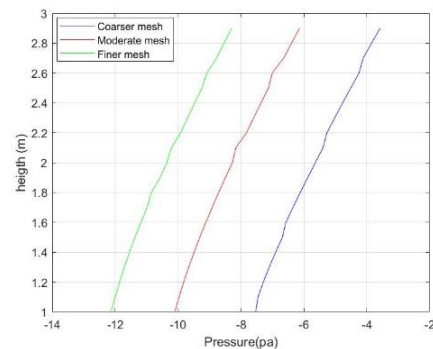**Fig 4.** Temperature comparison between three cases for sensitivity study

Fig 5. Pressure comparison between three cases for sensitivity study

From the figures shown above (Figs 4 and 5), it can be clearly seen that the temperature difference between the moderate and the finer cases was decreased from the coarser mesh. This is also the same for the pressure. The deviation of the quantities for the moderate case is not considerable compared to finer mesh, thus, the moderate mesh is selected for the further studies, which has the adequate accuracy and acceptable computational time.

3.2. Data validation

The basic case of the model for dry test (with no water mist activation) is compared with the model in ref [19] for the diesel pool fire with the peak HRR value equals to approximately 75 kw and the fuel pan size of 30 cm × 30 cm × 10 cm which is placed 20 cm above the floor. The room is exactly designed according to the characteristics mentioned in the reference. The comparison between the current model and the experimental study for the O2 concentration near the exhaust fan is displayed in Fig 6. The average difference between the results is below 1%. The comparison between the temperatures measured at the heights of 50cm, 150 cm, 250 cm, and 290 cm on a thermocouple tree with 140 cm offset from the central axis of the room in the corner. From Fig 7, it can be clearly seen that the obtained result from the designed model is in a good agreement with the data from the

experimental study. The deviation of the temperature at higher altitudes are much more than the lower part of the room and it is because of the difference between the damper design of the FDS model as a hole letting the fresh air being sucked into the room and the experimental one. The comparison is only carried out for the dry test (without water mist use). The HRR curve for validation case is shown in Fig. 8.
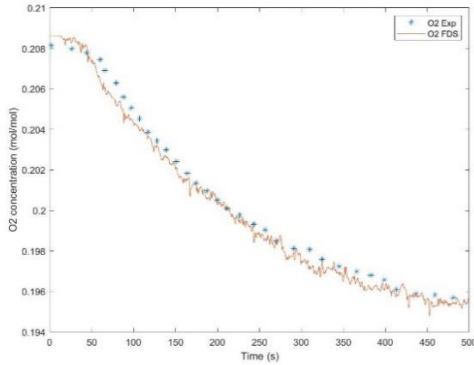

Fig. 6. Comparison of the O2 concentration between FDS (case I) and experimental results
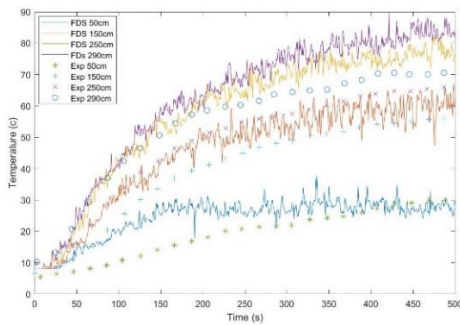
Fig. 7. Comparison of the temperature at the corner of the room at different height between FDS (case I) and experimental results
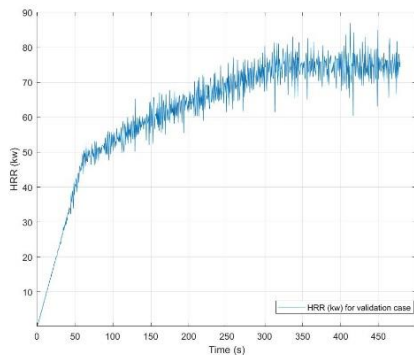
Fig 8. The HRR value of the validation model over time using the fire ramp in [19]

3.3. HRR and temperature fields

In FDS, according to [17], there are three basic principles for simulating water suppression namely, transporting the water droplets through the air, tracking the water along the solid surface, and predicting the reduction of the burning rate. The mass loss rate of the fuel and consequently HRR in suppression model of FDS is formulated as follows:

$$\dot{m}_f''(t) = \dot{m}_{f,0}'' e^{-\int k(t)dt} \tag{18}$$

In this equation, $\dot{m}_{f,0}''$ is the mass loss rate per unit area in case of dry test, and $k(t)$ is the function of the water mass per unit area which is defined as shown below:

$$k(t) = \alpha \dot{m}_w''(t) \tag{19}$$

The coefficient α is obtained experimentally. In FDS, the 'e_coefficient' can be introduced to see the reduction of burning rate in HRR curves after the nozzle activation.

The HRR evolution and the design fire curve are defined according to Reference [19] in FDS. For the water mist early applications, the nozzles are activated at 75s after ignition before HRR reaching to its peak value which is 75kw (the HRR at the time of water mist activation is around 50kw). For different cases with different obstacle scenarios, the HRR curves are plotted to compare the evolution after nozzle activation. For the water mist late applications, the nozzles are activated 190s after ignition. The HRR for these cases reaches to its peak value after 180s and then the free burning continues for 10s before the water mist is discharged. The following plots display the HRR evolution for different cases and the comparison between these cases.
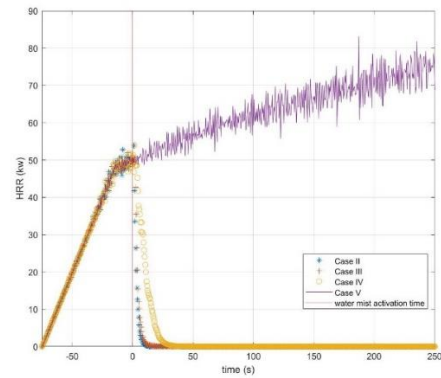

Fig. 9. HRR evolution for cases II to V

In Fig. 9, the HRR comparison for cases II to V (nozzle 1) is illustrated. The only case that the water mist system was unable to suppress the pool fire is case V in which the obstacle is 1m×1m in size and is located 800mm above the floor, although the fire size is small. In this case the fire pool is completely covered by the obstacle above, and the droplets are completely unable to reach to the fire plume or the surface. In addition, the oxygen concentration never drops below 15%. In case IV, the water mist is able to extinguish the fire around 25s after the nozzle activation. Cases II and III have almost the same curve and the burning rate decreases to 0 sharply after the activation. In case III, the obstacle is the smallest and mist droplets reach to the flame and the fire surface.
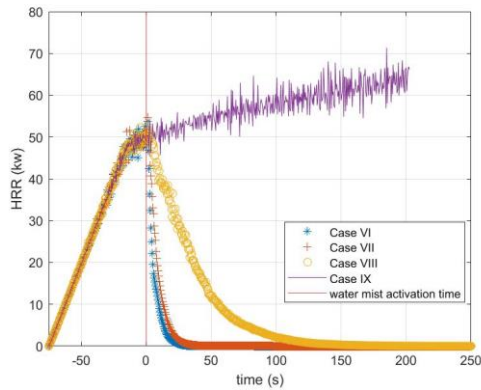
Fig. 10. HRR evolution for cases VI to IX

Fig. 10 shows the HRR evolution for cases using the second nozzle. As can be seen, the water mist system was unsuccessful to suppress the fire in the case which the obstacle is the biggest (case IX). In the other cases, the water mist system was able to completely extinguish the fire but compared to the first 4 cases using the nozzle 1, the extinguishing time is longer. For instance, for case VIII in which the obstacle characteristics are the same as case IV, the extinguishing time is almost doubled the time for case IV. In this regard, the first nozzle with finer droplets and higher pressure performed better compared to nozzle 2 regarding the shielded fire.
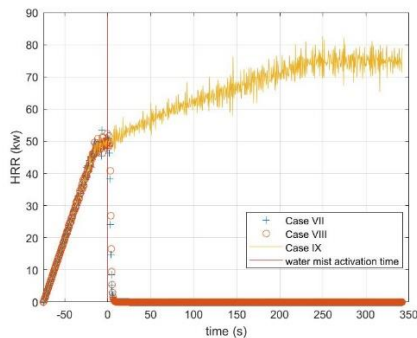

Fig. 11. HRR evolution for cases X to XII

The results for the HRR values of cases X to XII are shown in Fig. 11. In these cases, the obstacle is placed at the height of 1500mm above the floor. The water mist system is able to suppress the fire almost immediately for cases X and XI. For case XII, the water mist system failed to control the fire.
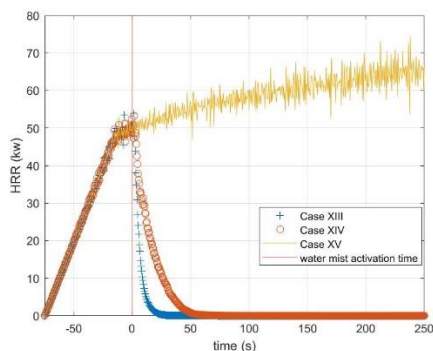

Fig. 12. HRR evolution for cases XIII to XV

Similar to Fig. 11, the simulations were carried out for cases XIII to XV using the second nozzle. As can be seen, nozzle 2 is also unable to suppress the shielded fire when the obstacle is the largest (case XV). However, it is clear that nozzle 1 performed better compared to nozzle when the obstacle is closer to the nozzle. The extinguishing time is lesser when using nozzle 1 for cases with the obstacle size of 25cm×25cm and 50cm×50cm.
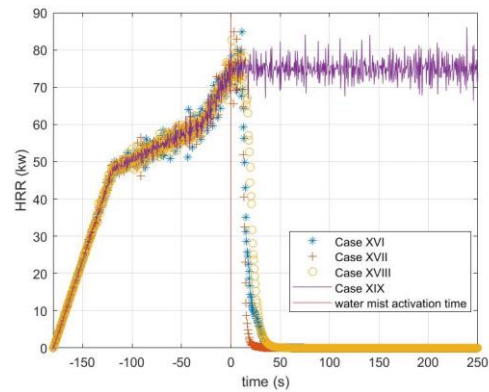

Fig. 13. HRR evolution for cases XVI to XIX

In order to analyze the performance of the water mist systems when the HRR is reached to its fully developed stage, several simulations are conducted letting the diesel burn for 190s and then the water mist will be activated. In Fig. 13, the comparisons of HRR curves between case XVI to XIX are displayed. In any cases except the one with the largest size of the obstacle, the nozzle 1 was able to suppress the fire completely below 50s. On the other hand, using nozzle 2, as shown in Fig. 14, is not as effective as nozzle 1 in terms of extinguishing time. For the case with the obstacle size of 50cm×50cm, nozzle 2 was able to extinguish the fire after almost 150s, while this time was around 40s using nozzle 1. Overall, it can be concluded that nozzle 1 with finer droplets had the better performance compared to nozzle 2 in extinguishing the fire considering the extinguishing time as the criterion.
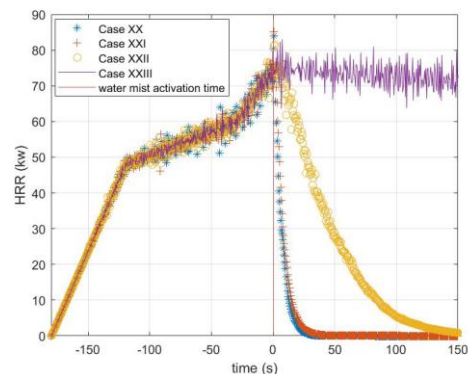

Fig. 14. HRR evolution for cases XX to XXIII

In this section, the temperature evolution of different cases and the comparisons are demonstrated. Due to the number of cases, only the most important

comparisons and temperature plots are mentioned here. The temperature values are obtained in 3 thermocouple trees, one in the center axis of the room above the fire, and the other two in the corners 1m away from the central axis. Only the temperature evolution on the corners is displayed here. The temperatures are measured at different heights from 50cm above the floor up to 290cm. Figs. 15 and 16 show the temperature evolution for cases using early application of nozzle 1. The temperature first decreases with the nozzle activation in case V (largest obstacle), but then increases rapidly up to 45°C. The other cases, as expected the temperature goes down sharply and stays at the constant value of the atmosphere temperature until the end of the simulation.
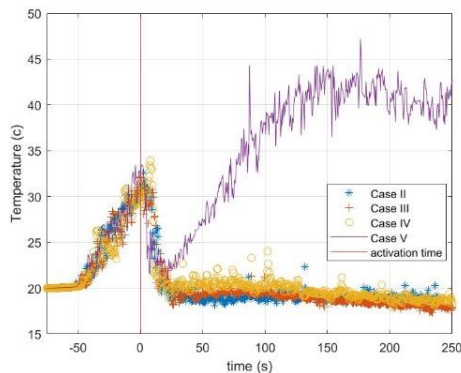

Fig. 15. Temperature evolution on the corner at the height 50cm for cases II to V

The same comparison has also been carried out for other cases. Figs. 17 and 18 represent the temperature evolution for cases VI to IX at 50cm and 290cm from the floor on the corner. In order to prevent the repetition, we ignore the explanation on other temperature plots as they have the same trend. Overall, both nozzles failed to control and decrease the temperature when the obstacle is the size of 1m×1m. However, in some cases, the nozzles were able to reduce the temperature even with the largest obstacle. For other cases with the obstacle size of 25cm×25cm and 50cm×50cm and for cases with no obstacle, both nozzles were able to control and reduce the temperature.
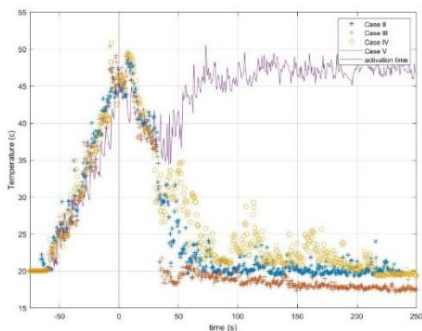

Fig. 16. Temperature evolution on the corner at the height 290cm for cases II to V
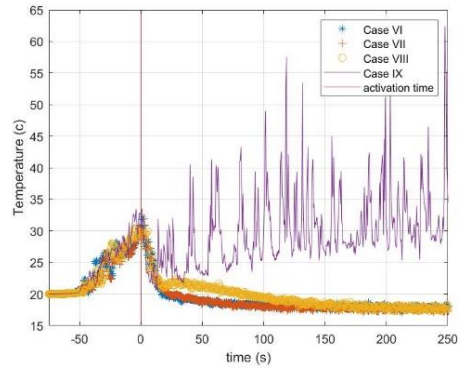

Fig. 17. Temperature evolution on the corner at the height 50cm for cases VI to IX

Fig. 18. Temperature evolution on the corner at the height 290cm for cases VI to IX

Fig. 19. Temperature evolution on the corner at the height 50cm for cases X to XII

Fig. 20. Temperature evolution on the corner at the height 290cm for cases X to XII

Fig. 21. Temperature evolution on the corner at the height 50cm for cases XIII to XV

Fig. 22. Temperature evolution on the corner at the height 290cm for cases XIII to XV

Fig. 23. Temperature evolution on the corner at the height 50cm for cases XVI to XIX
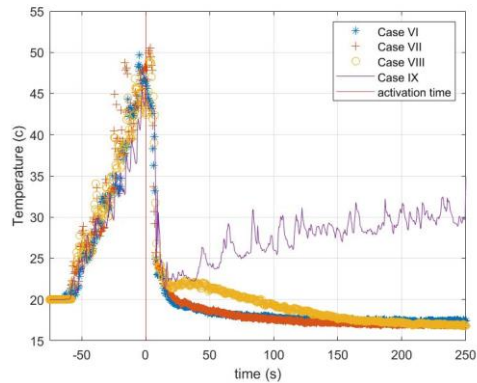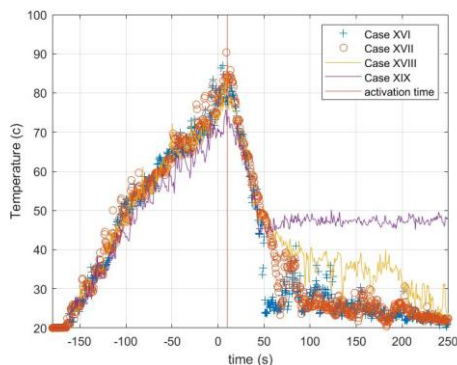

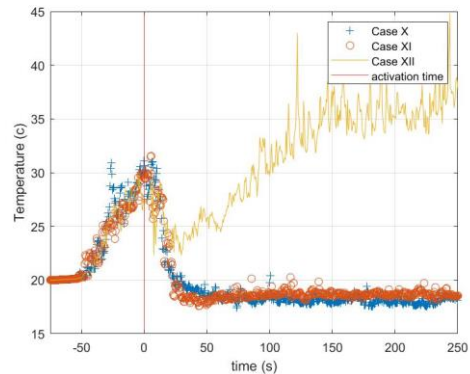**Fig. 24.** Temperature evolution on the corner at the height 290cm for cases XVI to XIX

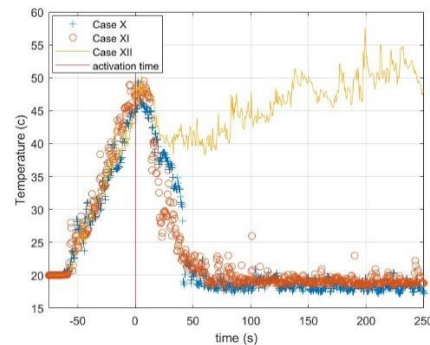**Fig. 25.** Temperature evolution on the corner at the height 50cm for cases XX to XXIII

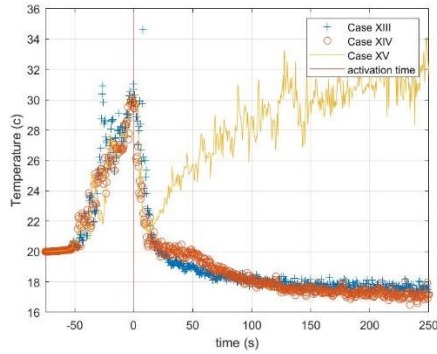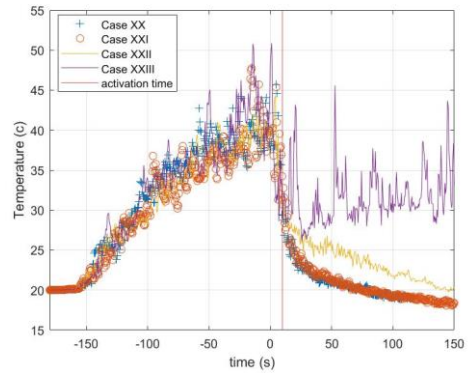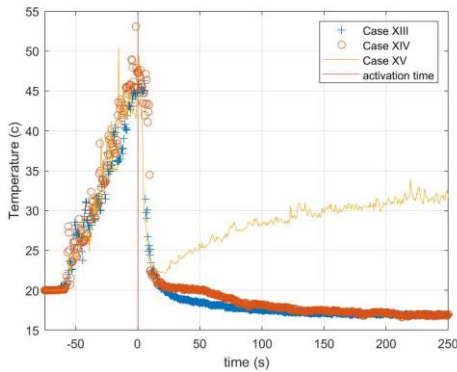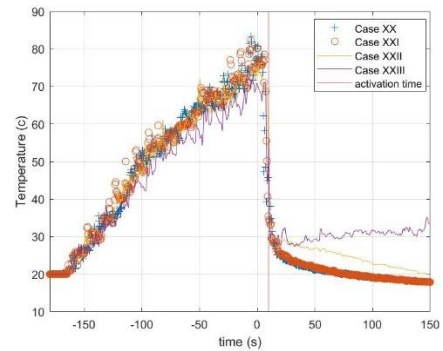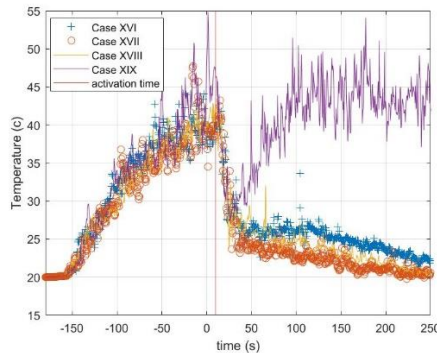**Fig. 26.** Temperature evolution on the corner at the height 290cm for cases XX to XXIII

The figures below represent the temperature and velocity contour plots at the plane y=2.15 in the middle of the compartment for all the cases. For the velocity contours, two plots including 1s before the water mist activation and 1s after the activation are displayed to compare the effect of the water droplets on the velocity field. As can be observed clearly, the velocity is the highest in the middle close to the nozzle after the activation. For the temperature contours, 4 different plots are displayed at different time for all cases including 1s before and after the activation, 5s and 10s after the activation. It can be seen that for the fully extinguished cases, the flame almost disappeared 10s after the activation and the temperature in the upper layers close to the ceiling is higher, and the air stratification can be clearly distinguished. For some cases, the water mist system is not able to suppress the fire and the fuel is still burning but is able to decrease the temperature range inside the enclosure a few seconds after the activation. In cases in which the obstacle is 1m×1m, the water mist fails to suppress or to control the fire because the obstacle is large enough to fully cover the fire and avoid reaching the droplets to the fire plume or flame.

Velocity contour at 75s, just before the nozzle activation for case II

Velocity contour at 76s, just after the nozzle activation for case II

Temperature contour at 75s, just before the nozzle activation for case II

Temperature contour at 76s, just after the nozzle activation for case II

Temperature contour at 80s, 5s after the nozzle activation for case II

Temperature contour at 85s, 10s after the nozzle activation for case II

Velocity contour at 75s, just before the nozzle activation for case III

Velocity contour at 76s, just after the nozzle activation for case III

Temperature contour at 75s, just before the nozzle activation for case III

Temperature contour at 76s, just after the nozzle activation for case III

10

Temperature contour at 80s, 5s after the nozzle activation for case III

Temperature contour at 85s, 10s after the nozzle activation for case III

Velocity contour at 75s, just before the nozzle activation for case IV

Velocity contour at 76s, just after the nozzle activation for case IV

Temperature contour at 75s, just before the nozzle activation for case IV

Temperature contour at 76s, just after the nozzle activation for case IV

Temperature contour at 80s, 5s after the nozzle activation for case IV

Temperature contour at 85s, 10s after the nozzle activation for case IV

Velocity contour at 75s, just before the nozzle activation for case V

Velocity contour at 76s, just after the nozzle activation for case V

Temperature contour at 75s, just before the nozzle activation for case V

Temperature contour at 76s, just after the nozzle activation for case V

Temperature contour at 80s, 5s after the nozzle activation for case V

Temperature contour at 85s, 10s after the nozzle activation for case V
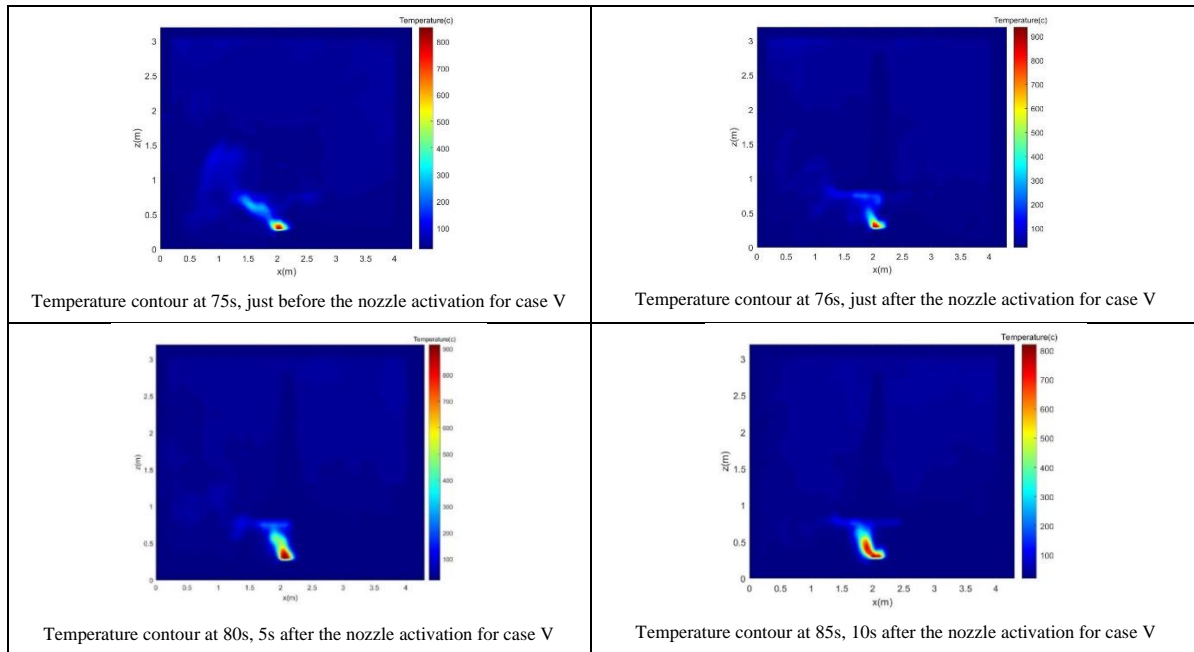
Fig. 27. Temperature and velocity contour plots for different cases, before and after the nozzle activation

4. Conclusion

In this study, the performance of two water mist systems (one low-pressure, one high-pressure nozzle) on the extinguishing performance of shielded fire in an enclosure is investigated using FDS. A 4.20 m×4.30m×3.05m enclosure is designed and modeled in FDS. The diesel pool fire with the HRR value of 75kw is placed in the middle of the room and obstacles with different sizes and different distance between the obstacle and the nozzle are designed above the fire to make it shielded. Two water mist systems including one high-pressure nozzle and one low-pressure nozzle are used to test their fire extinguishing performance. The following conclusions can be drawn:

- The FDS models were successfully validated by the available experimental data.
- The grid independency study was carried out to find out the appropriate cell size with an acceptable accuracy.
- Both nozzles were able to suppress the fire with no obstacle at a very short time.
- Both nozzles failed to suppress the shielded fire when the obstacle size was 1m×1m above the fire.
- Nozzle 1 performed better compared to nozzle 2 in extinguishing the shielded fire when the obstacle sizes were 50cm×50cm and 25cm×25cm.
- In successful cases of extinguishment, the temperature inside the enclosure decreased sharply until reached to the atmosphere temperature.
- As there was no direct contact between the droplets and the fuel surface or the flames, the dominant fire extinguishing mechanisms

were the oxygen displacement and the thermal radiation attenuation.

The authors would recommend researchers and engineers to perform more tests and simulations to investigate other available commercial water mist systems in case of shielded fires and to analyze the fire extinguishing mechanisms.

5. Acknowledgement

6. References

[1] N.F.P. Association, NFPA 750-Standard on water mist fire protection systems, (2006).

[2] G. Tian, H. Li, H. Xu, Y. Li, S.M. Raj, Spray characteristics study of DMF using phase doppler particle analyzer, SAE Int. J. Passeng. Cars-Mechanical Syst. 3 (2010) 948–958.

[3] Z. Wang, X. Wang, Y. Huang, C. Tao, H. Zhang, Experimental study on fire smoke control using water mist curtain in channel, J. Hazard. Mater. 342 (2018) 231–241. https://doi.org/https://doi.org/10.1016/j.jhazmat.2017.08.026.

[4] M. Gupta, A. Pasi, A. Ray, S.R. Kale, An experimental study of the effects of water mist characteristics on pool fire suppression, Exp. Therm. Fluid Sci. 44 (2013) 768–778. https://doi.org/https://doi.org/10.1016/j.expthermflusci.2012.09.020.

[5] J. Qin, W.K. Chow, Experimental Data on

Water Mist Suppression, Procedia Eng. 62 (2013) 868–877. https://doi.org/https://doi.org/10.1016/j.proeng.2013.08.137.

[6] L. Yinshui, J. Zhuo, W. Dan, L. Xiaohui, Experimental research on the water mist fire suppression performance in an enclosed space by changing the characteristics of nozzles, Exp. Therm. Fluid Sci. 52 (2014) 174–181. https://doi.org/https://doi.org/10.1016/j.expthermflusci.2013.09.008.

[7] C. Fan, R. Bu, X. Xie, Y. Zhou, Full-scale experimental study on water mist fire suppression in a railway tunnel rescue station: Temperature distribution characteristics, Process Saf. Environ. Prot. 146 (2021) 396–411. https://doi.org/https://doi.org/10.1016/j.psep.2020.09.019.

[8] Y.-M. Ferng, C.-H. Liu, Numerically investigating fire suppression mechanisms for the water mist with various droplet sizes through FDS code, Nucl. Eng. Des. 241 (2011) 3142–3148. https://doi.org/https://doi.org/10.1016/j.nucengdes.2011.06.002.

[9] Z. Wang, W. Wang, Q. Wang, Optimization of water mist droplet size by using CFD modeling for fire suppressions, J. Loss Prev. Process Ind. 44 (2016) 626–632. https://doi.org/https://doi.org/10.1016/j.jlp.2016.04.010.

[10] T. Sikanen, J. Vaari, S. Hostikka, A. Paajanen, Modeling and Simulation of High Pressure Water Mist Systems, Fire Technol. 50 (2014) 483–504. https://doi.org/10.1007/s10694-013-0335-8.

[11] Z. Lin, R. Bu, J. Zhao, Y. Zhou, Numerical investigation on fire-extinguishing performance using pulsed water mist in open and confined spaces, Case Stud. Therm. Eng. 13 (2019) 100402. https://doi.org/https://doi.org/10.1016/j.csite.2019.100402.

[12] J.R. Mawhinney, G.G. Back, Water mist fire suppression systems, in: SFPE Handb. Fire Prot. Eng., Springer, 2016: pp. 1587–1645.

[13] Y. Liu, X. Wang, T. Liu, J. Ma, G. Li, Z. Zhao, Preliminary study on extinguishing shielded fire with water mist, Process Saf. Environ. Prot. 141 (2020) 344–354.

https://doi.org/https://doi.org/10.1016/j.psep.2020.05.043.

[14] Y. Liu, Z. Fang, Z. Tang, T. Beji, B. Merci, The combined effect of a water mist system and longitudinal ventilation on the fire and smoke dynamics in a tunnel, Fire Saf. J. 122 (2021) 103351. https://doi.org/https://doi.org/10.1016/j.firesaf.2021.103351.

[15] C. Beihua, L. Guangxuan, H. Zhen, Extinction Limit of Diesel Pool Fires Suppressed by Water Mist, J. Fire Sci. 27 (2009) 5–26. https://doi.org/10.1177/0734904108095337.

[16] R.L. Alpert, Numerical modeling of the interaction between automatic sprinkler sprays and fire plumes, Fire Saf. J. 9 (1985) 157–163. https://doi.org/https://doi.org/10.1016/0379-7112(85)90003-7.

[17] K. McGrattan, S. Hostikka, R. McDermott, J. Floyd, C. Weinschenk, K. Overhold, Sixth Edition Fire Dynamics Simulator User 's Guide (FDS), NIST Spec. Publ. 1019. Sixth Edit (2020).

[18] G.P. Forney, Smokeview, A Tool for Visualizing Fire Dynamics Simulation Data, Volume I: User's Guide, NIST Spec. Publ. (2015) 1011–1017.

[19] A. Jenft, A. Collin, P. Boulet, G. Pianet, A. Breton, A. Muller, Experimental and numerical study of pool fire suppression using water mist, Fire Saf. J. 67 (2014) 1–12. https://doi.org/https://doi.org/10.1016/j.firesaf.2014.05.003.

13